Pergamon

Acta mater. 49 (2001) 3129–3142

Acta MATERIALIA

www.elsevier.com/locate/actamat

CRYSTAL STRUCTURE AND STABILITY OF COMPLEX PRECIPITATE PHASES IN Al–Cu–Mg–(Si) AND Al–Zn–Mg ALLOYS

C. WOLVERTON†

Ford Research Laboratory, MD3028/SRL, Dearborn, MI 48121-2053, USA

(Received 31 January 2001; received in revised form 29 May 2001; accepted 12 June 2001)

Abstract—We demonstrate how first-principles total energy calculations may be used to elucidate both the crystal structures and formation enthalpies of complex precipitates in multicomponent Al alloys. For the precipitates, *S*(Al–Cu–Mg), η' (Al–Zn–Mg), and *Q*(Al–Cu–Mg–Si), energetics were computed for each of the models of the crystal structures available in the literature allowing a critical assessment of the validity of the models. In all three systems, energetics were also calculated for solid solution phases as well as other key phases (e.g., equilibrium phases, GP zones) in each precipitation sequence. For both the *S* and η' phases, we find that recently proposed structures (based on electron microscopy) produce unreasonably high energies, and thus we suggest that these models should be re-evaluated. However, for all three precipitates, we find that structures based on X-ray diffraction refinements provide both reasonable energetics and structural parameters, and therefore the first-principles results lend support to these structural refinements. Further, we predict energy-lowering site occupations and stoichiometries of the precipitate phases, where experimental information is incomplete. This work suggests that first-principles total energy calculations can be used in the future as a complementary technique with diffraction or microscopy for studying precipitate structures and stabilities.

Keywords: Ab initio calculation; Aluminum alloys; Phase transformations; Precipitation

1. INTRODUCTION

Heat treatment of aluminum alloys is often employed in practice in order to strengthen the alloy via precipitation hardening. Precipitation microstructures improve the yield strength of the alloy because the precipitates act to impede dislocation motion through the material. The magnitude of the strengthening effect is, naturally, dependent on the microstructural morphology of the precipitates, which in turn is governed by the interfacial and strain energies of the precipitate/matrix system. These interfacial and strain energies are sensitive to the nature of the atomic-scale crystal structure of the precipitate phase, the matrix phase, and the interface between the two. Hence, a large amount of effort has gone into understanding the crystal structure of precipitate phases in aluminum-based alloys [1, 2].

However, despite decades of study, there are several commonly-occurring precipitate phases in multicomponent (ternary, quaternary, and higher order) aluminum alloys whose crystal structures are still the subject of significant controversy. In some cases, even the stoichiometry of the precipitate phase is not established. Notable among these controversial cases are:

1. the *S* (and/or *S*′) phase occurring in Al–Cu–Mg alloys;
2. the η' phase which occurs in Al–Zn–Mg alloys (with relatively low levels of Mg); and
3. the "ubiquitous" *Q* phase which occurs in a wide variety of quaternary Al–Cu–Mg–Si alloys.

In many of these alloys, the nature and structure of the Guinier–Preston (GP) zones formed in the early stages of aging are also a matter of debate.

The study of these multicomponent precipitate phases goes back more than 50 years, using techniques such as X-ray diffraction (XRD), electron microscopy, electron diffraction, and more recently, high-resolution electron microscopy (HREM), and both one- and three-dimensional atom probe techniques. The determination of precipitate crystal structure by diffraction experiments can be complicated by several factors: weak diffraction spots above the Al background scattering; significant overlap between precipitate and Al peaks; and low contrast between neighboring elements, such as Mg, Al, and Si. Despite the long history of this subject, the field is

† Fax: +1-313-322-7044.
E-mail address: cwolvert@ford.com (C. Wolverton)

1359-6454/01/$20.00
PII: S1359-6454(01)00229-4

still quite active, as evidenced by many recent papers (within the past 5 years) addressing the crystal structures and precipitation sequences in these systems: S/S' [3–13] η', [14–20] and Q [21–25]. The crystal structure of these three precipitate phases is the subject of the current paper. We also investigate GP zone orderings in Al–Cu–Mg and Al–Zn–Mg.

We show here how an existing technique may be brought to bear in a new way on problems of precipitate structure determination: first-principles total energy calculations based on density functional theory. While the XRD and HREM experimental efforts yield structural and chemical information, first-principles atomistic calculations give structural, chemical, and *energetic* information. Energetic information is not typically utilized in attempting to ascertain crystal structures, but it is reasonable to assume that the energies of precipitate phases are bounded above and below by the parent phase from which they transform, and the product phase into which they transform, respectively. These bounds place restrictions on the allowed energies of precipitate phases, and as we show here, they may be used to exclude many proposed structural models as "energetically unreasonable".

State-of-the-art first-principles calculations are particularly useful for obtaining the energetics of these precipitate phases for several reasons: The accuracy of *relative* energetics (e.g., the energy differences between two solid phases, as in a formation or mixing enthalpy) is quite high. As we show here, a comparison between first-principles and experimentally assessed CALPHAD (CALculation of PHAse Diagrams) data for Al-rich intermetallics yields a typical accuracy to within 2 kJ/mol for formation enthalpies. Also, first-principles methods are generally applicable to any elements in the periodic table and are not constrained by equilibrium thermodynamics. That is, these methods should be just as accurate for the energies of metastable states as they are for stable states. They are unbiased towards any particular structural model, making them a useful predictive tool for critically assessing various proposed precipitate structures.

In this paper, we apply arguments based on $T = 0$K energetics to the crystal structures of precipitates. However, precipitation is inherently a finite-temperature, kinetic process. So, the zero-temperature energetics do not yield a complete picture of the precipitation process, and hence one might wonder about the applicability of such an approach. As we show here, the energetic separation between various models of precipitate structures is very large (>10 kJ/mol), making several proposed crystal structure models unreasonably high in energy (e.g., higher in energy than either the solid solution phase or the GP zones phases from which the precipitates nucleate). Temperature-dependent effects (e.g., configurational and vibrational entropy) certainly will *quantitatively* effect the phase stability of these precipitates; however, entropic contributions are not likely to be large enough to qualitatively reverse these types of large energetic differences†.

2. METHODOLOGY

2.1. First-principles method

The first-principles calculations described utilize the plane wave pseudopotential method, as implemented in the highly efficient Vienna *ab initio* simulation package (VASP) [27–30], using ultrasoft pseudopotentials [31, 32]. In the vast majority of calculations reported here, the local density approximation (LDA) was employed, with the exchange-correlation functional of Ceperley and Alder [33, 34]. For a few calculations involving magnetic 3d elements Cr, Mn, Fe, Co, and Ni, spin-polarized calculations were performed using both the LDA as well as the generalized gradient approximation (GGA) of Perdew [35]. Tests were performed for the early transition elements, Sc and Ti, treating 3p electrons as valence versus core, with negligible differences between the two. All structures were fully relaxed with respect to volume as well as all cell-internal and -external coordinates. Convergence tests indicated that 237 eV (=17.5 Ry) was a sufficient cutoff to achieve highly accurate energy differences. Extensive tests of k-point sampling using both Monkhorst–Pack [36] and equivalent [37] k-point meshes (using from 2×2×2 to 16×16×16 grids) indicated that total energy differences were converged to well within ~1 kJ/mol.

2.2. Assessing the accuracy of first-principles formation enthalpies

Since we are attempting to critically evaluate various experimental measurements of crystal structures using a first-principles total energy method, assessing the accuracy of the computational approach is crucial, particularly in regard to formation enthalpies. The equilibrium formation enthalpy, $\Delta H^{eq}(A_pB_q)$, for a binary compound A_pB_q is given by the energy of A_pB_q relative to the composition-weighted average of the energies of the pure constituents each in their equilibrium crystal structures:

$$\Delta H^{eq}(A_pB_q) = E(A_pB_q) - [x_A E^{eq}(A) + x_B E^{eq}(B)] \quad (1)$$

where $E(A_pB_q)$, $E^{eq}(A)$ and $E^{eq}(B)$ are the energies (per atom) of the compound A_pB_q and constituents, A and

† A case has recently been found [26] in Al_2Cu where a very large and unexpected vibrational entropy can reverse a relatively modest (about 1 kJ/mol) energetic difference between two precipitate phases (θ and θ'). However, for the large energy differences found here, (often 10 kJ/mol) it is unlikely that entropic effects could have such an effect.

B, respectively, each relaxed to their equilibrium (zero-pressure) geometries. $x_A = p/(p + q)$ and $x_B = q/(p + q)$ are the concentrations of *A* and *B*, respectively. Analogous expressions apply for ternary and higher-order multicomponent compounds. We have computed the formation enthalpies of many Al-rich Al–*M* binary intermetallics in their equilibrium structures, for solutes across the 3d transition metal series *M*=Sc–Zn and for several elements commonly found in Al alloys, *M*=Mg, Si, and Sr†. Although there have been previous studies addressing the accuracy of first-principles calculations for describing formation enthalpies of intermetallics [38, 39] we wish to perform a systematic comparison for a wide range of aluminum-rich systems using a single method for all calculations. The calculated results are shown in Fig. 1. We chose these equilibrium intermetallics as a test case because their enthalpies of formation have been recently assessed and systematically compiled via a CALPHAD-type approach, whereby thermodynamic functions are fitted to experimental data, such as enthalpies, chemical potentials, and phase diagram information. This assessment has been detailed in the report of the COST 507 database [40]. These assessed values for the formation enthalpies are also shown in Fig. 1. As one can see, the agreement between the first-principles calculated formation enthalpies and the COST 507 values is excellent. Only the calculated Al_3Ti energy differs from the experimental value by as much as 4 kJ/mol, and all of the other calculated values are within 2 kJ/mol. Additionally, the errors appear to be systematic, as all of the first-principles calculated formation enthalpies are lower than the COST 507 values. One should note that this set of structures includes a wide, non-trivial range of stoichiometries, alloying elements, local coordinations, symmetries, and unit cell sizes (up to 52 atoms per unit cell). Thus, the excellent comparison between VASP calculations and the COST 507 database conclusively demonstrates that first-principles calculations of the type presented here are of the high accuracy necessary to critically assess the crystal structures of complex precipitate phases.

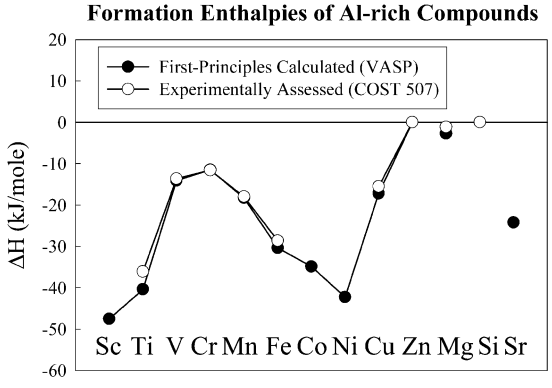

Fig. 1. Comparison of first-principles calculated and experimentally assessed (COST 507—Ref. [40]) formation enthalpies of Al-rich equilibrium compounds. The stoichiometry, Strukturbericht designation (if one exists), and Pearson symbol for the phases shown are: Al_3Sc ($L1_2$, cP4); Al_3Ti ($D0_{22}$, tI8); $Al_{45}V_7$ (mC104); $Al_{45}Cr_7$ (mC104); Al_6Mn ($D2_h$, oC28); $Al_{13}Fe_4$ (mC102); Al_9Co_2 ($D8_d$, mP22); Al_3Ni ($D0_{20}$, oP16); Al_2Cu (C16, tI12); Zn (hcp, A3, hP2); $Al_{12}Mg_{17}$ (A12, cI58); and Al_4Sr ($D1_3$, tI10).

For the magnetic elements *M*=Cr–Ni, spin polarized calculations were performed within both the LDA as well as the GGA for each of the constituents *M*, as well as the Al–*M* compounds in both the Al_9Co_2 and Al_6Mn structures. These GGA calculations were undertaken not so much because it was expected that the LDA versus GGA would make a significant difference for the Al-rich intermetallics, but rather since it is known that the magnetic *pure element* energy of equation (1) can by strongly affected by the choice of exchange correlation functional. Negligible differences were found between LDA and GGA results, except for the Al–Fe system. For the equilibrium $Al_{13}Fe_4$ phase, the LDA (GGA) formation enthalpy was found to be −36.0 (−30.4) kJ/mol, whereas the COST 507 database yields −28.6 kJ/mol. The somewhat larger disparity between LDA-calculated and experimental formation enthalpies in the Al–Fe system has also been found by Watson and Weinert [38]. We show here that use of the GGA largely removes this discrepancy for the $Al_{13}Fe_4$ compound. This sensitivity in the case of Fe to exchange-correlation functional is not surprising, since the LDA is known to produce the wrong magnetic and structural ground state (nonmagnetic fcc Fe), whereas GGA correctly gives ferromagnetic bcc Fe as the lowest-energy phase [41]. Consequently, all Al–*M* results shown in Fig. 1 are for the LDA, except Al–Fe which is GGA. All other results in this paper (none of which contain Fe) are LDA calculations, except where otherwise indicated.

2.3. Estimating multicomponent solution energies

In addition to the energetics of precipitate phases and equilibrium ordered compounds, it is also useful to describe the energetics of the "parent" solid solution phases. However, describing the energetics of solid solutions from first-principles is problematic since these calculations are currently limited to relatively small system sizes. This problem can be overcome by using the "special quasi-random structure" (SQS) approach [42], an efficient means to calculate random alloy properties within a small-unit-cell

† The pure element energies of equation 1 are calculated in their equilibrium, low-temperature structures with the exception of Cr and Mn, which have complex magnetic and structural ground states. Ferromagnetic bcc Cr and nonmagnetic fcc Mn were found to possess the lowest energies out of the simple bcc/fcc and non-/ferro-magnetic combinations, and hence these energies are used in evaluating the formation enthalpies. Also, as noted in the main text, the LDA (incorrectly) predicts nonmagnetic fcc Fe as a ground state, which was used as the pure element energy in the LDA Al–Fe calculations.

approach. In this paper, we use fully-relaxed, binary 16-atom SQSs (described in Appendix A) with stoichiometries A_3B and AB. The calculated formation enthalpies of the SQSs are given in Table 1. However, the SQS methodology is developed for binary systems, whereas we wish to ascertain the energetics of multicomponent solid solutions. For the extrapolation of binary energetics to multicomponent systems, we use a simple quadratic functional form for the composition dependence of the mixing energy:

$$\Delta H_{\mathrm{SS}}^{\mathrm{fcc}} = \sum_{I \neq J} \alpha_{IJ} x_I x_J \tag{2}$$

where x_I is the concentration of species I ($I = A, B, C, \ldots$) and α_{IJ} are constants. $\Delta H_{\mathrm{SS}}^{\mathrm{fcc}}$ is the "fcc-based" formation enthalpy of the solid solution phase. This quantity is a formation enthalpy, analogous to equation (1), except that the energy of the solid solution is evaluated with respect to the *pure constituents in the fcc structure*, rather than in their respective equilibrium structures. To obtain the formation enthalpy with respect to the equilibrium constituents, ΔH^{eq}, from the "fcc-based" formation enthalpy, ΔH^{fcc}, one simply has to add the composition-weighted energy required to promote each of the constituents from the equilibrium structure to the fcc structure:

$$\Delta H^{\mathrm{eq}} = \Delta H^{\mathrm{fcc}} + \sum_I x_I [E^{\mathrm{fcc}}(I) - E^{\mathrm{eq}}(I)]. \tag{3}$$

Table 1 gives the calculated values of ΔH^{eq}, ΔH^{fcc}, and $E^{\mathrm{fcc}} - E^{\mathrm{eq}}$ for all alloying elements and relevant binary combinations for the Al–Cu–Mg, Al–Zn–Mg, and Al–Cu–Mg–Si systems considered here.

Equation (2) is a simple, quadratic approximation to the actual composition-dependence of the solid solution energetics. We can use this functional form to interpolate the multicomponent energetics from a weighted average of binary solution phases. This interpolation is accomplished by fitting the constants α_{IJ} to SQS calculations of the corresponding binary random alloy energies. However, there is not a unique relationship between α_{IJ} and SQS energetics. For instance, one could rewrite equation (2) in terms of the equiatomic formation enthalpies by noting that $\alpha_{IJ} = 4\Delta H^{\mathrm{fcc}}(IJ)$. Alternatively, one could rewrite the expression in terms of binary energetics at other compositions, for example, $\alpha_{IJ} = [16/3]\Delta H^{\mathrm{fcc}}(I_3J)$. If the system of interest were truly described by a functional form like equation (2), either of these identifications would be equivalent. However, real alloy systems do not behave ideally, and first-principles calculations are not constrained by expressions such as equation (2). Thus, by fitting the coefficients α_{IJ} to various binary SQS energetics of various stoichiometries, we can test the robustness of such a simple description. In general, one would expect that fitting α_{IJ} with binary data as close as possible (in composition space) to the ternary composition of interest would yield the most accurate prediction.

As an example, consider the formation enthalpy of a solid solution with stoichiometry A_2BC. One could write this as:

$$\Delta H_{\mathrm{SS}}^{\mathrm{fcc}}(A_2BC) = \frac{1}{2}\Delta H_{\mathrm{SQS}}^{\mathrm{fcc}}(AB) + \frac{1}{2}\Delta H_{\mathrm{SQS}}^{\mathrm{fcc}}(AC) + \frac{1}{4}\Delta H_{\mathrm{SQS}}^{\mathrm{fcc}}(BC). \tag{4}$$

Table 1. First-principles (VASP) LDA-calculated formation enthalpies of SQSs[a]

System	Stoichiometry	$\Delta H_{\mathrm{SQS}}^{\mathrm{eq}}$	$\Delta H_{\mathrm{SQS}}^{\mathrm{fcc}}$	$E^{\mathrm{fcc}} - E^{\mathrm{eq}}$
Al–Cu	AlCu	−9.6	−9.6	
	Al_3Cu	−5.1	−5.1 (−5.7)	
Al–Zn	AlZn	+2.4	+1.1	
	Al_3Zn	+1.8	+1.2 (+1.6)	
Al–Mg	AlMg	+2.6	+1.9	
	Al_3Mg	+1.4	+1.0 (+0.7)	
Al–Si	AlSi	+15.7	−7.0	
	Al_3Si	+8.6	−2.7 (−2.9)	
Cu–Mg	CuMg	−1.9	−2.6	
Mg–Zn	MgZn	−4.1	−6.1	
Cu–Si	CuSi	+13.5	−9.2	
Mg–Si	MgSi	+7.0	−16.4	
Al				0.0
Cu				0.0
Zn				2.6
Mg				1.4
Si				45.4

[a] All energies are in kJ/mol. In all calculations, 16-atom SQSs and **k**-points equivalent to a 16×16×16 mesh were employed. (The description of the SQS structures are given in Appendix A.) The formation enthalpy with respect to the pure constituents in their equilibrium structures, $\Delta H_{\mathrm{SQS}}^{\mathrm{eq}}$ is given, as is the formation enthalpy with respect to the pure constituents in the fcc structure, $\Delta H_{\mathrm{SQS}}^{\mathrm{fcc}}$. In a few cases, GGA-calculated energies are shown (in parentheses) for comparison with the LDA results. Also, given is the energy required to promote the pure constituents from their equilibrium structures to the fcc structure.

Alternately, one could also write

$$\Delta H_{SS}^{fcc}(A_2BC) = \frac{2}{3}\Delta H_{SQS}^{fcc}(A_3B) + \frac{2}{3}\Delta H_{SQS}^{fcc}(A_3C) + \frac{1}{4}\Delta H_{SQS}^{fcc}(BC) \quad (5)$$

By comparing the two predictions of equations (4) and (5), one can get an estimate not only of $\Delta H_{SS}^{fcc}(A_2BC)$, but also of the error induced by assuming the solid solution form of equation (2).

The Al alloy solid solution phases which give rise to precipitates are typically not concentrated compositions, but rather dilute. Equation (2) gives a simple way to estimate the dilute heats of mixing:

$$\Delta H_{dilute}^{fcc}(AB_x) \equiv \left[\frac{d\Delta H^{fcc}}{dx}\right]_{x\to 0}. \quad (6)$$

Thus, for instance, the dilute heat of mixing of a ternary alloy with equal parts B and C can be written

$$\Delta H_{dilute}^{fcc}[A(BC)_x] = \frac{1}{2}\Delta H_{dilute}^{fcc}(AB_x) + \frac{1}{2}\Delta H_{dilute}^{fcc}(AC_x) \quad (7)$$

where

$$\Delta H_{dilute}^{fcc}(AB_x) = \frac{16}{3}\Delta H_{SQS}^{fcc}(A_3B). \quad (8)$$

It is worth emphasizing that the ternary energetics obtained in this way from binary calculations are simply estimates of the multicomponent solid solution phases, and should not be considered to have the same sort of accuracy as for ordered compounds, as in Fig. 1. A more complete and systematic description of binary Al alloy solid solutions from SQS calculations is given in Ref. [43].

3. STRUCTURE AND FORMATION ENTHALPIES OF Al–Cu–Mg PHASES: *S*/*S*′ PHASES, GPB ZONES, AND SOLID SOLUTION

The precipitation sequence formed upon heat treating Al–Cu–Mg has been studied for decades [3, 5–13, 44–49]. Al–Cu–Mg alloys have historically formed the basis of many alloys used in aerospace and other applications, and have been suggested as an alternative to 6*xxx* series alloys for use in automotive body panels (see, e.g., Refs. [6, 7]) In alloys close to the pseudo-binary Al–Al_2CuMg compositions, the sequence is [44]:

Solid solution→GPB zones→*S*

In the early stages of aging, coherent precipitates form [called Guinier–Preston–Bagaryastskii (GPB) zones], although the precise structure of these zones is not known [44, 45]. There has been quite a bit of recent discussion in the literature about the initial stages of decomposition which precede the formation of GPB zones, and the origins of the age hardening associated with these stages [8–12, 3, 13]. As for the latter stages of precipitation, Bagaryastskii reported [45] two intermediate phases *S*″ and *S*′ that are slightly distorted versions of the equilibrium Al_2CuMg *S* phase, with different matrix-precipitate coherence. Many authors have noted that only slight differences in lattice parameters differentiate the *S*′ phase from the equilibrium phase *S*, but otherwise their structures are the same. For the purposes of this paper, we do not distinguish between *S*″, *S*′, and S, but rather consider only the equilibrium *S* phase.

3.1. *S* phase

Several structural models have been proposed for the Al_2CuMg *S* phase† [2, 5, 46–48]. By XRD, Perlitz and Westgren (PW) [46] found a model for *S* which is centered orthorhombic with 16 atoms per conventional unit cell. Mondolfo [2] suggested an analogous model to PW with slightly different lattice parameters. Very recently, Radmilovic, Kilaas, Dahmen, and Shiflet (RKDS) [5] have re-evaluated the structure of *S* phase precipitates using quantitative HREM. These authors found that of the existing models for *S*, only the PW model gave results consistent with their HREM images and electron diffraction results. However, by comparing measured and simulated HREM images, RKDS proposed yet another model for Al_2CuMg (*S*), which is identical to the PW model, except that Cu and Mg atoms are interchanged.

We have calculated the enthalpies of formation of both the PW [46] and RKDS [5] models of Al_2CuMg (*S*). The results are given in Table 2. The first-principles calculation using the PW model yields a reasonable (negative) formation enthalpy, in good agreement with the measured formation enthalpy of Notin *et al.* [49] However, upon interchange of Cu and Mg atoms (the RKDS model), the energy is raised by a large amount, resulting in a positive formation enthalpy. This suggests that the RKDS model for *S* is unstable with respect to phase separation into the constituent metals, Al, Cu, and Mg. Thus, the first-principles results of Table 2 support the validity

† The structural models of *S*″ given by Cuisiat *et al.* [48] and that of *S*′ from Yan *et al.* [47], yield an unexpected precipitate density which is only about half that of the aluminum matrix. However, recent XRD work [4] undertaken to clarify the controversy between the various models of *S*, *S*′, and *S*″ supported the models of Perlitz and Westgren [46] and Mondolfo [2]. Hence, we do not consider the models of Cuisiat *et al.* or Yan *et al.* here.

Table 2. First-principles calculated (VASP) formation enthalpies ΔH^{eq} (kJ/mol) of Al_2CuMg phases: solid solution, GPB zones, and S/S' [using both the models of Perlitz and Westgrin (PW) [46] and Radmilovic *et al.* (RKDS) [5]]. Also shown is the measured formation enthalpy of S

Phase	VASP	Experiment
Al_2CuMg solid solution	$\sim -4.0 \pm 1$	
GPB zones ($Al_1Mg_1Al_1Cu_1$ [100] superlattice)	−9.1	
Al_2CuMg S (PW model)	−19.4	
Al_2CuMg S (RKDS model)	+16.4	
Al_2CuMg S		−15.8 [49]

of the XRD-derived PW model, and suggest that the HREM-derived RKDS model should be re-evaluated.

Table 3 gives the calculated structural parameters of the S phase, compared with the measured values of Perlitz and Westgren. The lattice constants are in reasonable agreement with experiment, and the cell-internal positions are in excellent agreement with experiment, as is typical in first-principles calculations. This agreement further suggests that the PW model is correct. On the other hand, the RKDS model results in extremely large distortions from these structural positions. Thus, calculations using the proposed Cu/Mg interchange in the RKDS model yield both energetic and structural information that is inconsistent with experimental observations.

3.2. GPB zones

In order to further elucidate the energetics of decomposition in the Al–Cu–Mg system, we next turn to the coherent GPB zones. Estimating the energetics of GPB zones is not straightforward, since the structure of these zones is not known. Recently, first-principles calculations were used to evaluate the structure and equilibrium shape of GP zones in binary Al–Cu alloys [50, 51]. These calculations were performed by mapping energetics of several fcc-based Al–Cu configurations along with coherency strain energies onto a mixed-space cluster expansion, which was subsequently used in a Monte Carlo approach to predict large-scale (250 000-atom) coherent alloy morphologies. By using such an approach, one can *predict* the energy-minimizing morphologies of coherent precipitates, whether or not the precipitate structure is known experimentally. However, this type of mixed-space cluster expansion approach has not yet been extended to ternary systems. Therefore, we instead estimate the energetics of coherent Al_2CuMg configurations more directly by performing first-principles calculations for a wide variety of fcc-based superlattices: $Al_2Cu_1Mg_1$ and $Al_1Mg_1Al_1Cu_1$ each stacked along [100], [111], [110], [210], [311], as well as an $L1_2$-based Al_2CuMg ternary structure. From these 11 fcc-based configurations, we find a clear energetic preference for the $Al_1Mg_1Al_1Cu_1$ superlattice along [100] (structure shown in Fig. 2) with a formation enthalpy of $\Delta H = -9.1$ kJ/mol. (The range of formation enthalpies for these structures was −9.1 to +0.6 kJ/mol with the second-lowest energy fcc-based structure, $Al_2Cu_1Mg_1$ along [100], having a formation enthalpy of −4.6 kJ/mol). While this sampling of 11 fcc-based configurations is by no means a full ternary "ground state search" [52] of all possible fcc-based states, it does give an indication of the possible preferred stacking sequence of the GPB zones as well as an estimate of their energetics. The energy of the $Al_1Mg_1Al_1Cu_1$ [100] superlattice is given in Table 2.

The structure of the low-energy $Al_1Mg_1Al_1Cu_1$ superlattice is related to a binary $Al_1Al_1Al_1Cu_1$ [100] superlattice with one of the Al planes replaced by Mg. The binary and ternary versions of this superlattice are shown in Fig. 2. Recent first-principles calculations [50] have predicted that this binary $Al_1Al_1Al_1Cu_1$ [100] superlattice corresponds to a metastable Al_3Cu phase which should appear in the *coherent* Al–Cu phase diagram (i.e., under the constraint of considering only coherent, fcc-based configurations). The two types of GP zones (GP1 and GP2) in Al–Cu both correspond to precipitation of this Al_3Cu phase with a size-dependent transition in the equilibrium shape from GP1 zones at small precipitate sizes to GP2 at ca 100–150 Å [50]. In Al–Cu–Mg alloys, there are reports of two types of GPB

Table 3. Comparison of first-principles calculated (VASP) and experimental structural properties of S-Al_2CuMg using the model of Perlitz and Westgren [46][a]

Property	VASP	Experiment [46]
a	3.93	4.00–4.03
b	9.12	9.23–9.30
c	6.99	7.08–7.18
V	250.3	263.6–265.7
$(y,z)_{Al}$	(0.356, 0.055)	(0.356, 0.056)
$(y,z)_{Cu}$	(0.780, 0.250)	(0.778, 0.250)
$(y,z)_{Mg}$	(0.066, 0.250)	(0.072, 0.250)

[a] Lattice constants (a, b, c) are in Å, V is the unit cell volume (in Å^3), and $(x, z)_i$ are the cell-internal positions for atom i.

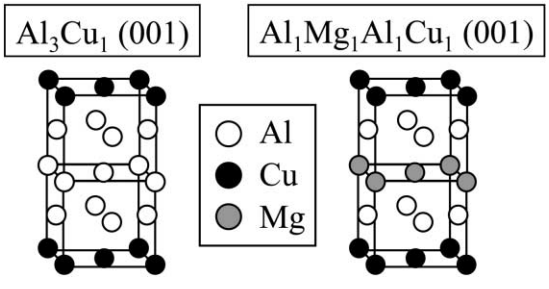

Fig. 2. Low-energy coherent configurations in the Al–Cu and Al–Cu–Mg systems found by first-principles calculations. Shown is the $Al_1Al_1Al_1Cu_1$ [100] superlattice, predicted to be a "coherent" ground state in Al–Cu (see Ref. [50]) and the low-energy $Al_1Mg_1Al_1Cu_1$ [100] superlattice found here.

zones (often called GPB and GPB2), in analogy to the GP1/GP2 zones in binary Al–Cu [44]. Additionally, there are suggestions that the GPB zones correspond to monolayers of solute atoms on [100] planes [3], and that GPB2 zones are a three-dimensional (possibly ordered) version of GPB containing both Cu and Mg [44]. (Other authors have suggested that the GPB zones correspond to [210] planes of solute atoms [2, 45]. Our calculations include the $Al_2Cu_1Mg_1$ [210] superlattice, which corresponds to the Bagaryastskii model of S''. We find that this superlattice is much higher in energy than the [100] superlattices.) In analogy with the proposed explanation for GP1/GP2 in Al–Cu [50], it is possible that the both the GPB and GPB2 zones are due to a single phase in the coherent Al–Cu–Mg phase diagram, with the GPB zones corresponding to monolayers due to the GPB/matrix interfacial energy, and GPB2 zones develop an ordering along [100], like the structure shown in Fig. 2. This explanation is highly speculative, since we have only considered a limited number of possible configurations, although a more complete first-principles investigation of the ternary Al–Cu–Mg coherent phase stability (analogous to that of Ref. [50] for Al–Cu) would be interesting.

3.3. Al–Cu–Mg solid solution

The supersaturated solid solution phase gives rise to the precipitate phases in the first place. The Al–Cu–Mg alloys in which precipitation is observed contain relatively dilute amounts of Cu and Mg (a few atomic percent or less); however, each of the other phases considered in this system was at Al_2CuMg stoichiometry. For a consistent comparison with these phases, we have estimated the energy of an Al_2CuMg solid solution phase: the solid solution energetics were estimated using a ternary solution model in conjunction with binary SQS calculations, as explained in Section 2.3. We used the Al–Cu, Al–Mg, and Cu–Mg SQS energetics given in Table 1. Using the equiatomic SQSs and equation (4), we find $\Delta H(Al_2CuMg) = -4.2$ kJ/mol. Alternatively, using the Al_3Cu and Al_3Mg SQSs along with equation (5) gives $\Delta H(Al_2CuMg) = -3.0$ kJ/mol. We can also estimate the dilute heat of mixing for the quasi-binary Al–Al_2CuMg using equations (7) and (8). We find $\Delta H^{eq}_{dilute}[Al(CuMg)_x] = -10.2$ kJ/mol of solute atoms. Linearly extrapolating this to Al_2CuMg composition yields $\Delta H(Al_2CuMg) = -5.1$ kJ/mol. Thus, from these three values of $\Delta H(Al_2CuMg)$ we conclude that the errors inherent in this sort of method yield $\Delta H(Al_2CuMg) \sim -4.0 \pm 1$ kJ/mol, which is the value we list in Table 2.

From the solid solution, GPB, and S-phase energetics in Table 2, one can see that the general sequence of the precipitation in these alloys is correctly preserved in the energetics of Al_2CuMg (provided that the PW model is adopted for the S phase): $\Delta H(\text{Solid solution}) > \Delta H(\text{GPB}) > \Delta H(S)$.

4. Al–Mg–Zn: η, η' PHASES, GP ZONES, AND SOLID SOLUTION

Additions of Mg and Zn to Al form the basis of many 7*xxx* series high-strength, heat treatable alloys. Consequently, the precipitation sequence in Al–Zn–Mg alloys has been the subject of much interest [1, 2, 20, 16, 15, 17–19, 53]. For relatively high Zn:Mg ratios, this sequence (see the recent review in Ref. [20]) is:

$$\text{Solid solution} \rightarrow \text{GP zones} \rightarrow \eta' \rightarrow \eta.$$

Upon aging, the solid solution gives way to (two types of) GP zones, then to a semicoherent metastable phase η', and finally to the equilibrium $MgZn_2$ (η) phase. If the Zn:Mg ratio is too high, another equilibrium phase, Mg_2Zn_{11}, can also appear.

4.1. Equilibrium $MgZn_2$ (η) and Mg_2Zn_{11} phases

Since the crystal structures of the η phase and Mg_2Zn_{11} are unambiguously known, we begin with calculations of these phases. Table 4 shows the calculated and observed structural parameters of the $MgZn_2$ η phase. The η phase is hexagonal, with space group $P6_3/mmc$ and 12 atoms per unit cell. Although the agreement between theory and experiment is good, we note that the lattice parameters have a ~3–4% error relative to experiment, larger than is typical from first-principles methods. The error in lattice constant for this Zn-rich compound is somewhat expected however, since it is known that LDA calculations of the lattice parameter of hcp-Zn show a large error (e.g., ~3% in Ref. [54]). However, the calculated *relative* structural properties of $MgZn_2$, such as the c/a ratio of η, or the fractional cell-internal positions are in excellent agreement with experimental observations. The calculated formation enthalpy of η is within 4 kJ/mol of the COST 507 database [40], and just as in Fig. 1, the first-principles value is more negative than the assessed value. We also computed the energetics and structural properties of the Zn-rich equilibrium compound, Mg_2Zn_{11} (not shown in Table 4). This compound is cubic with space group $Pm\bar{3}$

Table 4. Comparison of first-principles calculated (VASP) and experimental structural and energetic properties of η-$MgZn_2$[a]

Property	VASP	Experiment [64]
a	5.04	5.22
c	8.28	8.57
c/a	1.64	1.64
V	182.4	202.2
$(x, y, z)_{Mg}$	(0.333, 0.667, 0.062)	(0.333, 0.667, 0.063)
$(x, y, z)_{Zn1}$	(0.000, 0.000, 0.000)	(0.000, 0.000, 0.000)
$(x, y, z)_{Zn2}$	(0.831, 0.661, 0.250)	(0.830, 0.661, 0.250)
ΔH^{eq}	−15.6	−11.8 (Ref. [49])

[a] Lattice constants (a, b, c) are in Å, V is the unit cell volume (in Å^3), $(x, z)_i$ are the cell-internal positions for atom i, and ΔH^{eq} is the formation enthalpy, in kJ/mol.

and 39 atoms per unit cell. The calculated formation enthalpy of this phase, −8.2 kJ/mol, is also a few kJ/mol lower than the COST 507 database value, −5.7 kJ/mol.

4.2. η' phase

The high strength of Al–Zn–Mg alloys and the pronounced hardening response to heat treatment is generally associated with the η' phase [20]. Hence, this is a well-studied but still controversial metastable phase. Significant disagreements exist regarding the crystal structure and even composition of this phase: η' is commonly assumed to have the composition $MgZn_2$, in analogy with the equilibrium η phase. Recent three-dimensional atom probe investigations of η' have found Zn:Mg ratios varying from 1.2 to 1.4, depending on the composition of the alloy [16]. However, structural models proposed [55, 14, 56] for the η' phase all contain significantly higher Zn:Mg ratios than this, with some ratios higher than that of $MgZn_2$. Also, some investigations find evidence for Al in the structure of this phase [14, 55].

There exist several models of the crystal structure of η': in an early model, Gjonnes and Simensen [56] proposed an orthorhombic structure of η' with stoichiometry $MgZn_2$. However, it has subsequently become accepted that η' is hexagonal with $a = 4.96$ Å and $c = 14.02$ Å, and is structurally related to the equilibrium η phase. Using XRD of single crystals, Auld and Cousland [55] deduced a structural model of η' with an approximate composition $Mg_4Zn_{11}Al$. Although this model was challenged by the XRD work of Regnier *et al*. [57], Auld and Cousland subsequently responded to this criticism [58] and maintained that their model was correct. Recently, Li *et al*. [14] have investigated η' precipitates by means of HREM, and have found a structural model with stoichiometry $Mg_2Zn_{5-x}Al_{2+x}$, which is distinct from either that of Gjonnes and Simensen [56] or Auld and Cousland [55]. We have performed first-principles calculations of the three distinct models of η' proposed by Gjonnes and Simensen [56], Auld and Cousland [55] and Li *et al*. [14]. The results are shown in Fig. 3.

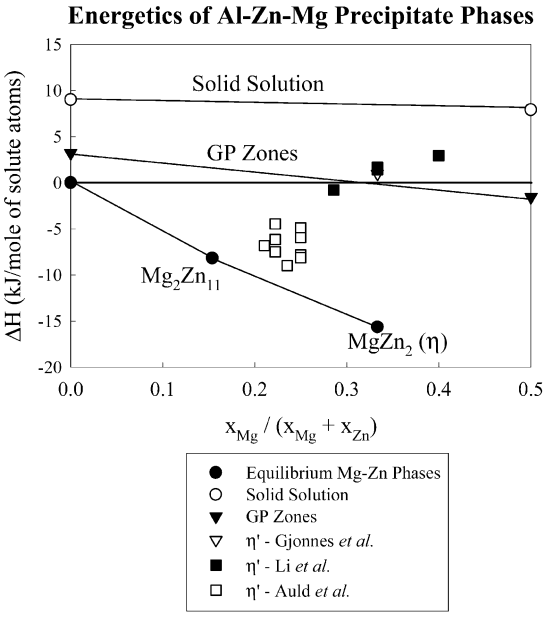

Fig. 3. First-principles calculated energetics in the Zn-rich corner of the Al–Zn–Mg system. Shown are formation enthalpies of the equilibrium phases [$MgZn_2$ (η) and Mg_2Zn_{11}], a simple model of the energetics of the GP zones and dilute solid solutions, and several models (with varying site occupations) of the structure of η': Gjonnes *et al*. [56], Li *et al*. [14], and Auld *et al*. [55]. To compare energetics of structures with varying Al content, but fixed Mg/Zn ratio, all energies are given in terms of kJ/*mol of solute atoms*. The model of Auld *et al*. clearly provides the most reasonable energetics, between that of the GP zones and the equilibrium phases.

4.2.1. Gjonnes and Simensen model. The orthorhombic model of Gjonnes and Simensen contains complete crystal structure information with all sites fully occupied. The calculated energy for this model is quite high and even slightly positive, indicating an instability with respect to phase separation. Since the Al–Zn–Mg system possesses a solid solution formation enthalpy which is positive, it is conceivable that the η' precipitate phase could have a positive formation enthalpy and still be lower in energy than the solid solution. However, since η' is thought to be structurally related to the equilibrium η phase (which has a strong negative formation enthalpy), we consider it extremely unlikely that η' has a positive formation enthalpy, and therefore we assert that the first-principles results do not support the model of Gjonnes and Simensen.

4.2.2. Li et al. model. For the structural refinements given by both Li *et al*. and Auld and Cousland, some sites were given either partial or mixed occupations. Therefore, we investigate several different occupations of atoms in each of these sites in order to fully assess the energetics of these structural models. The structural model of Li *et al*. [14] is $P\bar{6}$ and contains eight symmetry-inequivalent sites: two each with occupation by Mg, Zn, and Al, and two others which can be occupied either by Zn or Al. These latter two sites are, in the notation of Ref. [14], Zn3 and Zn5 sites (Wyckoff position 2*g*). We have performed total energy calculations with five different arrangements of Zn/Al on these Zn3 and Zn5 sites: Zn on both sites (yielding a stoichiometry $Mg_2Zn_5Al_2$), Al on both sites ($Mg_2Zn_3Al_4$), Al (Zn) on Zn3 (Zn5) or vice versa ($Mg_2Zn_4Al_3$), and finally Al on one each of the two Zn3/Zn5 sites in the cell ($Mg_2Zn_4Al_3$). (It should be noted that this last configuration breaks the $P\bar{6}$ symmetry.) As in the case of the Gjonnes and Simensen model, the model of Li *et al*. yields high-energy results for all of the Zn/Al arrangements considered. All of these formation enthalpies are either positive or only slightly negative, and just as in the

case of the Gjonnes and Simensen model, the first-principles energetics do not support the recently-proposed η' model of Li *et al.*

4.2.3. Auld and Cousland model. The model of Auld and Cousland is $P\bar{6}m2$ and also contains eight symmetry-inequivalent positions: two are fully occupied by Mg and two by Zn. However, there are two sites (which Auld and Cousland specify as "A" and "E") as occupied two-thirds by Zn and one-third by vacancies, and two other sites ("G" and "H") with half Zn and half Al. We have considered more than a dozen configurations of Zn, Al, and vacancies on these four sites. The specifics of the considered configurations are not reported here, but we give the trends we found from comparing the total energies of these various configurations: there is an energetic preference for Al (as opposed to Zn) on the "G" and "H" sites. On the "A" and "E" sites, the strongest energetic preference is for these sites to be *fully occupied* by Zn (i.e., with no vacancies). However, if these sites are not fully occupied by Zn, it was found that a partial occupation by Al is energetically preferable, compared with a partial occupation by vacancies. It is worth noting that Auld and Cousland observed scattering power from these "A" and "E" sites which was less than that of Zn atoms, but higher than Al or Mg, and hence concluded that they were not fully occupied by Zn. They considered the possibility of Al on these sites to be unlikely based on simple bond-length arguments. However, our total energy calculations have shown that Al on these sites is preferable to vacancies, although full Zn occupation is the lowest energy. Thus, our lowest-energy structure (with Al on "G" and "H" and Zn on "A" and "E") is a slight modification of the original Auld and Cousland model, with stoichiometry $Mg_4Zn_{13}Al_2$. The results for all configurations based on the Auld and Cousland model are shown in Fig. 3. Of the three models proposed in the literature for η', this is the only one which yields "appropriate" energetics, that is, strongly negative formation enthalpies of the same magnitude as that of η. Thus, *the first-principles results support the validity of the Auld and Cousland model for* η'.

Table 5 gives the calculated and experimental structural information for the η' phase, using the model of Auld and Cousland. The calculations of the bulk, unstrained structure yield lattice constants which deviate from the observed values by an unusually large amount. To this point, all calculations in this paper have been unstrained, that is, all cell vectors and volume are completely relaxed to their energy-minimizing values. However, diffraction studies [55, 53] have found that the lattice parameters of η' are constrained by the matrix of Al with the following orientation relationships: $c_{\eta'} = 6d_{111\mathrm{Al}} = 2\sqrt{3}a_{\mathrm{Al}}$ and $a_{\eta'} = 2d_{112\mathrm{Al}} = \sqrt{6}/2a_{\mathrm{Al}}$. We have repeated the calculations of the first-principles predicted $Mg_4Zn_{13}Al_2$ structure straining the lattice vectors according to the observed constraints, but otherwise relaxing all cell-internal positions. With these constraints, the calculated cell vectors now differ from experiment only because of the small underestimate of the calculated lattice parameter of aluminum, a_{Al}. This strained calculation also reveals the energetic effect of the lattice parameter constraints: The ΔH of η' rises by 2 kJ/mol when the cell vectors are strained. Also, by comparing the lattice parameters of the strained and unstrained calculations, we see that the η' precipitates in Al–Zn–Mg alloys are under very large strains: a 5.7% tensile strain along $c_{\eta'}$ and a 3.4% compressive strain along $a_{\eta'}$.

4.3. Al–Zn–Mg GP zones

To explore the energetics of the Al–Zn–Mg precipitation sequence more fully, we also investigated the energetics of GP zones. As described above (for Al–Cu–Mg), the energies of ternary Al–Zn–Mg GP zones were estimated by considering a variety of fcc-based superlattices. The same five superlattice orientations were considered for $Al_1Mg_1Zn_1Mg_1$ and $Al_2Mg_1Zn_1$ superlattices. In this system, additional calculations were performed for $Al_4Mg_1Zn_2Mg_1$ superlattices. This more complicated stacking was considered based on the ordered tendencies in the Al–Zn, Al–Mg, and Mg–Zn binaries: the Al–Zn system shows a miscibility gap, indicating that Zn and Al prefer to cluster, whereas Al–Mg and Mg–Zn both order. Thus, one might speculate that an energetically favored superlattice would entail Zn planes which are clustered and only in contact with Mg. The Mg planes, on the other hand, could be in contact with both Zn and Al. Therefore, we selected the $Al_4Mg_1Zn_2Mg_1$ stacking sequence to satisfy these two criteria. From the first-principles calculations of the 16 fcc superlattices considered, we find that the $Al_4Mg_1Zn_2Mg_1$ superlattice along [311] is lower in energy than any of the considered $Al_1Mg_1Zn_1Mg_1$ or $Al_2Mg_1Zn_1$ stackings, or the $L1_2$-based structure. The energy of this [311] superlattice is shown in Fig. 3 as an estimate of the GP zones energy for Mg:Zn ratio 1:1. For the Zn-rich GP zones, recent first-principles work [59] in corroboration with precipitation experiments in Al–Zn has shown that the lowest-energy fcc-based coherent state is phase-separation between Al and Zn along [111]. Thus, we have calculated the coherency strain energy (as defined in Ref. [59]) along [111] for fcc-Zn, shown in Fig. 3 as an estimate of the energetics of GP zones for zero Mg content. For intermediate compositions, we simply linearly interpolate between these two points, to give a rough scale of the GP zone energetics.

4.4. Al–Zn–Mg solid solution

Estimates of the solid solution phases were also made, using binary SQSs combined with the ternary solid solution model as described above. Since the various models of η' and η involve a range of different compositions, we compute the dilute heat of for-

Table 5. Comparison of first-principles calculated (VASP) and experimental structural and energetic properties of η' (Al–Zn–Mg), using the model of Auld and Cousland [55][a]

Property	Occupation		VASP		Experiment [55]
	VASP $Mg_4Zn_{13}Al_2$	Ref. [55] $Mg_4Zn_{11}Al_1$	Unstrained	Strained $c_{\prime\prime} = 6d_{111Al}$ $a_{\prime\prime} = 3d_{112Al}$	Strained $c_{\prime\prime} = 6d_{111Al}$ $a_{\prime\prime} = 3d_{112Al}$
a			5.04	4.87	4.96
c			13.03	13.77	14.02
c/a			2.58	2.83	2.83
V			286.2	282.8	298.7
ΔH^{eq}			−8.1	−6.1	
$(x, y, z)_A$	Zn	$\frac{2}{3}$Zn + $\frac{1}{3}\square$	(0.503, 0.497, 0.000)	(0.501, 0.499, 0.000)	(0.500, 0.500, 0.000)
$(x, y, z)_B$	Mg	Mg	(0.000, 0.000, 0.120)	(0.000, 0.000, 0.120)	(0.000, 0.000, 0.113)
$(x, y, z)_C$	Zn	Zn	(0.333, 0.667, 0.160)	(0.333, 0.667, 0.160)	(0.333, 0.667, 0.148)
$(x, y, z)_D$	Mg	Mg	(0.667, 0.333, 0.197)	(0.667, 0.333, 0.202)	(0.667, 0.333, 0.183)
$(x, y, z)_E$	Zn	$\frac{2}{3}$Zn + $\frac{1}{3}\square$	(0.165, 0.835, 0.322)	(0.166, 0.834, 0.321)	(0.166, 0.833, 0.296)
$(x, y, z)_F$	Zn	Zn	(0.667, 0.333, 0.408)	(0.667, 0.333, 0.410)	(0.667, 0.333, 0.398)
$(x, y, z)_G$	Al	$\frac{1}{2}$Zn + $\frac{1}{2}$Al	(0.000, 0.000, 0.500)	(0.000, 0.000, 0.500)	(0.000, 0.000, 0.500)
$(x, y, z)_H$	Al	$\frac{1}{2}$Zn + $\frac{1}{2}$Al	(0.333, 0.667, 0.500)	(0.333, 0.667, 0.500)	(0.333, 0.667, 0.500)

[a] Lattice constants (a, c) are in Å, V is the unit cell volume (in Å^3), $(x, y, z)_i$ are the cell-internal positions for site i, using the site notation in Ref. [55]. ΔH^{eq} is the formation enthalpy, in kJ/mol. The energy-minimizing site occupations for the first-principles calculations are distinct from those of Ref. [55], resulting in stoichiometries of $Mg_4Zn_{13}Al_2$ and $Mg_4Zn_{11}Al_1$ for first-principles and experiment, respectively. Shown are calculated results for the unstrained cell, as well as calculated structure with lattice vectors strained by the observed orientation relationships.

mation as a function of Zn:Mg ratio, from equations (6), (8) and (2). The SQS energetics yield $\Delta H_{\text{dilute}}(\text{AlZn}_x) = +9.0$ kJ/mole of solute and $\Delta H_{\text{dilute}}(\text{Al(ZnMg)}_x) = +7.9$ kJ/mole of solute. These dilute formation energies are shown in Fig. 3.

To summarize the energetics of Fig. 3, the ordering of $T = 0$ formation enthalpies correctly follows the observed precipitation sequence (when the Auld and Cousland model is adopted for η'):
$\Delta H(\text{Solid solution}) > \Delta H(\text{GP}) > \Delta H(\eta') > \Delta H(\eta)$.

5. Al–Cu–Mg–Si: *Q* PHASE

The quaternary "*Q* phase" is found in a wide variety of Al–Cu–Mg–Si alloys, for example, 6*xxx* series Al–Mg–Si alloys with Cu additions [24], or Al–Si–Cu casting alloys containing Mg, such as Al 319 [60]. Despite its common presence in these alloys, relatively little is known about the *Q* phase compared to other commonly-occurring precipitates. Even the stoichiometric composition of *Q* varies from one study to another, reported as $Al_4Cu_2Mg_8Si_7$ [61], $Al_5Cu_2Mg_8Si_6$ [62] and $Al_4Cu_1Mg_5Si_4$ [2]. Another variant of the *Q* phase has been reported in Al–Mg–Si alloys [25] without Cu in the structure. It is possible, but unsubstantiated, that the different reported compositions are due to off-stoichiometry in the single-phase field of *Q* in the quaternary phase diagram (as opposed to a line compound).

Most of the structural studies of the *Q* phase have yielded lattice constants and symmetry information, but not the specificity of a crystal structure. The symmetry is generally acknowledged to be hexagonal, with lattice constants ca $a = 10.35-10.40$ Å, $c = 4.02-4.05$ Å, and 21 atoms per unit cell. Only Arnberg and Aurivillius [61] have proposed a (partial) crystal structure for *Q*: these authors find that the *Q* phase is related to the Th_7S_{12} structure, with Si replacing Th, Al+Mg replacing *S*, and Cu located at voids of the structure. These authors used XRD to determine the structural information and did not differentiate between Al and Mg in their refinement. They therefore specified the composition as $Al_xCu_2Mg_{12-x}Si_7$.

In an effort to elucidate the crystal structure and phase stability of *Q*, we perform first-principles calculations based on the model of Arnberg and Aurivillius [61]. The atomic positions of the structure are given in Table 6. The positions labeled M_1, M_2, M_3, and M_4 are those which contain either Al or Mg. We perform a series of calculations based on this structure, systematically vary the Al/Mg content and site occupations within these four sites in order to ascertain the lowest-energy state. The total number of Al/Mg sites in the $Al_xCu_2Mg_{12-x}Si_7$ model is 12. Since each of the "*M*" sites in the Arnberg and Aurivillius model has a degeneracy of three, we begin with three Al atoms (and nine Mg atoms) making a stoichiometry $Al_3Cu_2Mg_9Si_7$. The formation enthalpies of the four possible unit cells formed by placing all three Al atoms in each of the *M* sites is shown in Fig. 4. There is a strong energetic preference for all three Al to go

Table 6. Comparison of first-principles calculated (VASP) and experimental structural and energetic properties of Q-$Al_xCu_2Mg_{12-x}Si_7$[a]

Property	VASP		Experiment [61]
	$Al_3Cu_2Mg_9Si_7$ Unstrained	Strained $c_Q = a_{Al}$, $a_Q = \frac{\sqrt{26}}{2}a_{Al}$	$Al_4Cu_2Mg_8Si_7$
a	10.25	10.14	10.39
c	3.93	3.98	4.02
V	357.7	353.8	375.8
$(x, y, z)_{M_1}$	(0.252, 0.006, 0.000)	(0.253, 0.007, 0.000)	(0.242, 0.002, 0.000)
$(x, y, z)_{M_2}$	(0.634, 0.138, 0.000)	(0.634, 0.139, 0.000)	(0.633, 0.140, 0.000)
$(x, y, z)_{M_3}$	(0.798, 0.996, 0.500)	(0.797, 0.994, 0.500)	(0.788, 0.992, 0.500)
$(x, y, z)_{M_4}$	(0.379, 0.857, 0.500)	(0.379, 0.857, 0.500)	(0.379, 0.859, 0.500)
$(x, y, z)_{Cu_1}$	(0.333, 0.667, 0.000)	(0.333, 0.667, 0.000)	(0.333, 0.667, 0.000)
$(x, y, z)_{Cu_2}$	(0.667, 0.333, 0.500)	(0.667, 0.333, 0.500)	(0.667, 0.333, 0.500)
$(x, y, z)_{Si_1}$	(0.000, 0.000, 0.000)	(0.000, 0.000, 0.000)	(0.000, 0.000, 0.000)
$(x, y, z)_{Si_2}$	(0.584, 0.857, 0.000)	(0.584, 0.858, 0.000)	(0.582, 0.862, 0.000)
$(x, y, z)_{Si_3}$	(0.421, 0.131, 0.500)	(0.420, 0.131, 0.500)	(0.416, 0.132, 0.500)
ΔH^{eq}	$x = 3$: −17.7 $x = 4$: −15.6	−17.5	

[a] Lattice constants (a, b, c) are in Å, V is the unit cell volume (in Å^3), $(x, y, z)_i$ are the cell-internal positions for atom i, and ΔH^{eq} is the formation enthalpy in kJ/mol. Shown are the calculated results for the unstrained cell, as well as calculated structure with lattice vectors strained by the coherency relationships given in Ref. [24].

into the M_1 sites (denoted "3 M_1"). Also, energetics were calculated for several $Al_3Cu_2Mg_9Si_7$ configurations with three Al atoms on a mixture of the four sites. None of these structures had a lower energy than "3 M_1".

Since the reported stoichiometries of Q, $Al_4Cu_2Mg_8Si_7$ and $Al_5Cu_2Mg_8Si_6$, have more than three Al atoms in the unit cell, we have also explored the energetics of additional Al in the structure. Shown in Fig. 4 are the energetics of configurations with four Al atoms in the unit cell, making the stoichiometry $Al_4Cu_2Mg_8Si_7$. With three of the Al atoms already accounted for in M_1 sites, there are only three possible positions (M_2, M_3, and M_4) for the fourth Al. We find that the M_4 site is very slightly energetically preferred for $x = 4$ Al stoichiometries. However, all considered configurations have formation energies higher than that of the lowest energy $Al_3Cu_2Mg_9Si_7$ state (with three M_1 Al atoms).

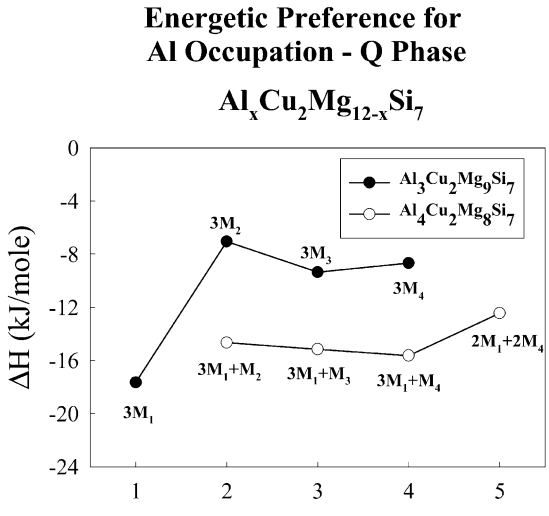

Fig. 4. Formation enthalpies of Q-phase $Al_xCu_2Mg_{12-x}Si_7$ unit cells using the structural model of Arnberg and Aurivillius. Shown are several $Al_3Cu_2Mg_9Si_7$ and $Al_4Cu_2Mg_8Si_7$ cells with the Al atoms in the four sites M_i given in Table 6. The M_1 site is the energetically-preferred site for Al occupation. Once the M_1 sites are fully occupied by Al, the M_4 site is the next most energetically preferred.

To examine the $Al_5Cu_2Mg_8Si_6$ stoichiometry, we begin with the lowest energy $Al_4Cu_2Mg_8Si_7$ cell, and systematically replace one Si atom with an Al, for each of the three Si sites. The energies of these configurations (not shown in Fig. 4) demonstrate that the Si_1 site is strongly preferred, relative to Si_2 or Si_3 for Al atoms. In all cases though, this $Al_5Cu_2Mg_8Si_6$ cell has a higher formation enthalpy than either the $Al_4Cu_2Mg_8Si_7$ or $Al_3Cu_2Mg_9Si_7$ cells.

We have also considered configurations with fewer than three Al atoms, $x = 2$, 1, and 0 (all Al atoms in the M_1 sites). The results of all of the above calculations, plotted as a function of Al content are shown in Fig. 5. Clearly, the $x = 3$ composition represents the lowest-energy state. Either adding additional Al to this structure, or replacing Al with Mg in this structure results in a $T = 0$ energy penalty. From these calculations, we propose a new stoichiometric composition of the Q phase, $Al_3Cu_2Mg_9Si_7$, and assert that observed compositions with higher Al content than this are due to off-stoichiometry in the phase field of Q at finite temperatures. From these calculations, then, we provide an experimentally testable prediction: the composition of Q obtained as a precipitate in Al–Cu–Mg–Si alloys should be temperature-dependent (in contrast to the prediction of Q as a stoichiometric line compound, which would yield a temperature-independent composition). This off-stoichi-

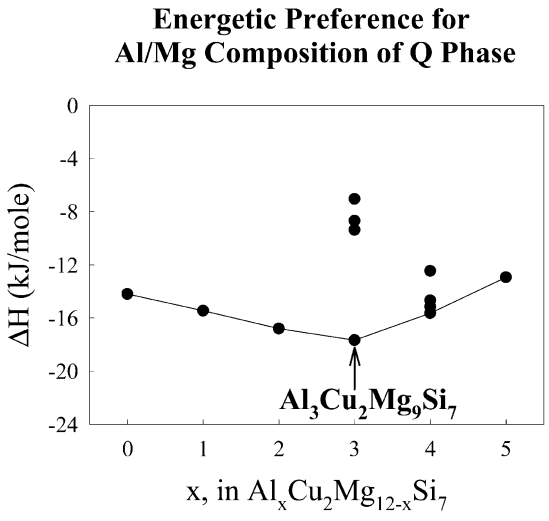

Fig. 5. Formation enthalpies of Q-phase $Al_xCu_2Mg_{12-x}Si_7$ unit cells as a function of x. The lowest-energy structure is for $x = 3$, or $Al_3Cu_2Mg_9Si_7$ stoichiometry.

ometry also could explain the differing compositions reported by various authors, and should provide a basis for a more accurate treatment of Q in computational thermodynamics approaches where Q is currently treated as a line compound [63].

Although Arnberg and Aurivillius were unable to distinguish Al and Mg in their refinements, they did offer some suppositions about their site occupations [61]. Since the M_1 sites are 12-fold coordinated whereas the M_2, M_3, and M_4 sites are 15-fold coordinated, they assumed that the M_1 sites would be occupied by Al. Based on bond-length arguments, they also supposed that any additional Al atoms in the structure would prefer the M_4 sites, and that M_2 and M_3 sites would be exclusively occupied by Mg. Remarkably, although these arguments are quite speculative, in each case they are confirmed by our first-principles calculated energetics.

In addition to the equilibrium form of Q, a coherent version of the same phase has been noted, with coherency relations [24]: $c_Q = a_{\mathrm{Al}}$, $a_Q = (\sqrt{26}/2)a_{\mathrm{Al}}$. We have also performed calculations of our $Al_3Cu_2Mg_9Si_7$ cell with lattice vectors strained by these coherency relations (Table 6). The equilibrium lattice parameters are already quite close to these constrained values, thus demonstrating only a very small strain (and hence a very small energetic effect of coherency). Our calculations indicate that the coherent version of Q is under a 1.1% compressive strain along a and a 1.3% tensile strain along c.

6. SUMMARY

We have demonstrated the utility of first-principles calculations in elucidating the crystal structures and phase stability of several complex, multicomponent precipitate phases in Al alloys: S (Al–Cu–Mg); η' (Al–Zn–Mg); and Q (Al–Cu–Mg–Si). A critical assessment of the accuracy of first-principles formation enthalpies in a wide variety of ordered Al-rich intermetallics shows that the calculated energetics are in excellent quantitative agreement (to within 2 kJ/mol) with experimentally assessed databases. Since there is no reason to expect first-principles methods to be any less accurate for multicomponent, or metastable ordered phases, we expect that the first-principles methods are capable of discriminating between the various crystal structure models proposed for S, η', and Q.

In addition to the metastable precipitate phases, we also calculate the energetics of the equilibrium phases, solid solutions, and coherent GP zones in each system. The multicomponent solid solution mixing energies are obtained using a simple quadratic function of composition, with coefficients fit to energies of binary SQSs. Coherent GP zone energetics are estimated from a series of fcc-based superlattice calculations, using a wide range of superlattice stackings and orientations.

6.1. Al–Cu–Mg

The first-principles calculated energetics support the XRD model of the Al_2CuMg S phase given by Perlitz and Westgren. The calculated properties of S agree well with experiment for lattice constants, cell-internal parameters, and formation enthalpies. Calculations of a recently proposed structure for S, deduced from HREM, yield a very high energy, and therefore we suggest that this model be revisited. The energies of fcc-based superlattices show a low energy…Al/Cu/Al/Mg…superlattice along (100), which may be an indication of the preferred type of ordering in GPB zones, although a more detailed study of this problem is required to make these conclusions more definitive. Estimates of the ternary solid solution phase yield energetics consistent with the observed precipitation sequence in these alloys: $\Delta H(\text{Solid solution}) > \Delta H(\text{GPB}) > \Delta H(S)$.

6.2. Al–Zn–Mg

Calculations of three distinct models of the η' phase crystal structure demonstrate that the Auld and Cousland model yields reasonable energetics in this system, whereas the other two models do not. Additionally, we have found the energetically-preferred occupations for partially occupied sites in the Auld and Cousland model, which lead to a new, proposed low-energy stoichiometry for this phase: $Mg_4Zn_{13}Al_2$. The equilibrium phases ($MgZn_2$ and Mg_2Zn_{11}), for which the crystal structures are known, yield calculated structural and energetic properties in good agreement with experimental values, giving confidence in the calculated properties of the metastable η' phase. Energetics of 16 fcc superlattices considered show a complicated stacking sequence is lowest in energy, again underscoring the need for a more thorough study of fcc-based configurations to deduce the structure of GP zones in the Al–Zn–Mg

system. Combining the calculated mixing enthalpies of the ternary solid solution to the calculations of equilibrium, metastable, and GP zone phases, gives energetics in line with the observed precipitation sequence: ΔH(Solid solution) $>\Delta H$(GP) $>\Delta H(\eta')$ $>\Delta H(\eta)$.

6.3. Al–Cu–Mg–Si

First-principles calculations of the quaternary *Q* phase were performed using the model of Arnberg and Aurivillius. The calculated structural properties are in good agreement with observed lattice constants and cell-internal positions. Additionally, we provide formation enthalpies of this phase to serve as predictions for future experimental investigations, as we are unaware of any observed energetics for this phase. The site occupation of Al versus Mg is not given in the Arnberg and Aurivillius model, but our calculations clearly demonstrate the energetic site preference for these two species, yielding a new energy-minimizing stoichiometry for this phase: $Al_3Cu_2Mg_9Si_7$. Observations of additional Al content in this phase could be an indication of off-stoichiometry in the *Q* single-phase-field, since these observations are typically for *Q* phase precipitates in Al-rich alloys.

Acknowledgements—The author gratefully acknowledges many useful discussions with Drs J. Allison, W. Donlon and R. Jahn.

REFERENCES

1. Hatch, J. E., *Aluminum: Properties and Physical Metallurgy*. American Society of Metals, Ohio, 1998.
2. Mondolfo, L. F., *Aluminum Alloys—Structure and Properties*. Butterworths, London, 1976.
3. Charai, A., Walther, T., Alfonso, C., Zahra, A. -M. and Zahra, C. Y., *Acta Mater.*, 2000, **48**, 2751.
4. Perez-Landazabal, J. I., No, M. L., Madariaga, G. and San Juan, J., *J. Mater. Res.*, 1997, **12**, 577.
5. Radmilovic, V., Kilaas, R., Dahmen, U. and Shiflet, G. J., *Acta Mater.*, 1999, **47**, 3987.
6. Ratchev, P., Verlinden, B., de Smet, P. and van Houtte, P., *Acta Mater.*, 1998, **46**, 3523.
7. Ratchev, P., Verlinden, B., de Smet, P. and van Houtte, P., *Mater. Trans. JIM*, 1999, **40**, 34.
8. Ringer, S. P., Hono, K., Polmear, I. J. and Sakurai, T., *Appl. Surf. Sci.*, 1996, **94/95**, 253.
9. Ringer, S. P., Hono, K., Sakurai, T. and Polmear, I. J., *Scripta Mater.*, 1997, **36**, 517.
10. Zahra, A. M., Zahra, C. Y., Alfonso, C. and Charai, A., *Scripta Mater.*, 1998, **39**, 1553.
11. Ringer, S. P., Caraher, S. K. and Polmear, I. J., *Scripta Mater.*, 1998, **39**, 1559.
12. Somoza, A., Dupasquier, A., Polmear, I. J., Folegati, P. and Ferragut, R., *Phys. Rev. B*, 2000, **61**, 14454.
13. Reich, L., Ringer, S. P. and Hono, K., *Phil. Mag. Lett.*, 1999, **79**, 639.
14. Li, X. Z., Hansen, V., Gjonnes, J. and Wallenberg, L. R., *Acta Mater.*, 1999, **47**, 2651.
15. Ferragut, R., Somoza, A. and Tolley, A., *Acta Mater.*, 1999, **47**, 4355.
16. Maloney, S. K., Hono, K., Polmear, I. J. and Ringer, S. P., *Scripta Mater.*, 1999, **41**, 1031.
17. Stiller, K., Warren, P. J., Hansen, V., Angenete, J. and Gjonnes, J., *Mater. Sci. Engng*, 1999, **A270**, 55.
18. Yamamoto, A., Minami, K., Ishihara, U. and Tsubakino, H., *Mater. Trans. JIM*, 1998, **39**, 69.
19. Chinh, N. Q., Kovács, Z., Reich, L., Székely, F., Illy, J. and Lendvai, J., *Z. Metallkd.*, 1997, **88**, 607.
20. Lendvai, J., *Mater. Sci. Forum*, 1996, **217-222**, 43.
21. Cayron, C. and Buffat, P. A., *Acta Mater.*, 2000, **48**, 2639.
22. Barlow, I. C., Rainforth, W. M. and Jones, H., *J. Mater. Sci.*, 2000, **35**, 1413.
23. Miao, W. F. and Laughlin, D. E., *Metal. Mater. Trans.*, 2000, **31A**, 361.
24. Chakrabarti, D. J., Cheong, B. -K. and Laughlin, D. E., in *Automotive Alloys II, Proc. TMS Annual Meeting in San Antonio, TX, Feb. 1998*, ed. S. K. Das. TMS, Warrendale, 1998, pp. 27–44.
25. Sagalowicz, L., Lapasset, G. and Hug, G., *Phil. Mag. Lett.*, 1996, **74**, 57.
26. Wolverton, C. and Ozolins, V., *Phys. Rev. Lett.*, 2001, **86**, 5518.
27. Kresse, G. and Hafner, J., *Phys. Rev. B*, 1993, **47**, 558.
28. Kresse, G. Thesis, Technische Universität Wien 1993.
29. Kresse, G. and Furthmüller, J., *Comput. Mat. Sci.* , 1996, **6**, 15–50.
30. Kresse, G. and Furthmüller, J., *Phys. Rev. B*, 1996, **54**, 11169.
31. Vanderbilt, D., *Phys. Rev. B*, 1990, **41**, 7892.
32. Kresse, G. and Hafner, J., *J. Phys.: Condens. Matt.*, 1994, **6**, 8245.
33. Ceperley, D. M. and Alder, B. J., *Phys. Rev. Lett.*, 1980, **45**, 566.
34. Perdew, J. P. and Zunger, A., *Phys. Rev. B*, 1981, **23**, 5048.
35. Perdew, J. P., in *Electronic Structure of Solids 1991*, Vol. 11, ed. P. Ziesche and H. Eschrig. Akademie Verlag, Berlin, 1991.
36. Monkhorst, H. J. and Pack, J. D., *Phys. Rev. B*, 1976, **13**, 5188.
37. Froyen, S., *Phys. Rev. B*, 1989, **39**, 3168.
38. Watson, R. E. and Weinert, M., *Phys. Rev. B*, 1998, **58**, 5981.
39. Watson, R. E., Weinert, M., Davenport, J. W. and Fernando, G. W., *J. Phase Equil.*, 1994, **15**, 273.
40. Fries, S. G. and Jantzen, T., *Thermochim. Acta*, 1998, **314**, 23.
41. Amador, C., Lambrecht, W. R. L. and Segall, B., *Phys. Rev. B*, 1992, **46**, 1870.
42. Zunger, A., Wei, S. -H., Ferreira, L. G. and Bernard, J. E., *Phys. Rev. Lett.*, 1990, **65**, 352.
43. Wolverton, C., Unpublished data.
44. Silcock, J. M., *J. Inst. Met.*, 1960, **89**, 203.
45. Bagaryatskii, A., *Zh. Tech. Fiz.*, 1948, **18**, 424.
46. Perlitz, H. and Westgren, A., *Ark. Chem. Miner. Geol.*, 1943, **16B**, 13.
47. Yan, J., Chunzhi, L. and Minggao, Y., *J. Mater. Sci. Lett.*, 1990, **9**, 421.
48. Cuisiat, F., Duval, P. and Graf, R., *Scripta Met.*, 1984, **18**, 1051.
49. Notin, M., Dirand, M., Bouaziz, D. and Hertz, J., *C.R. Acad. Sci. Paris*, 1986, **302**, 63.
50. Wolverton, C., *Phil. Mag. Lett.*, 1999, **79**, 683.
51. Wolverton, C., *Model. Simul. Mater. Sci.*, 2000, **8**, 323.
52. Ceder, G., Garbulsky, G. D., Avis, D. and Fukuda, K., *Phys. Rev. B*, 1994, **49**, 1.
53. Park, J. K. and Ardell, A. J., *Metall. Trans.*, 1983, **14A**, 1957.
54. Fast, L., Ahuja, R., Nordstrom, L., Wills, J. M., Johansson, B. and Eriksson, O., *Phys. Rev. Lett.*, 1997, **79**, 2301.
55. Auld, J. H. and Cousland, S. McK., *J. Australian Inst. Met.*, 1974, **19**, 194.
56. Gjonnes, J. and Simensen, Chr. J., *Acta Met.*, 1970, **18**, 881.
57. Regnier, P. C., Bouvaist, J. and Simon, J. P., *J. Appl. Cryst.*, 1982, **15**, 590.
58. Auld, J. H. and Cousland, S. McK., *J. Appl. Cryst.*, 1985, **18**, 47.

59. Müller, S., Wang, L. -W., Zunger, A. and Wolverton, C., *Phys. Rev. B*, 1999, **60**, 16448.
60. Jahn, R., Donlon, W. and Allison, J., Private communication.
61. Arnberg, L. and Aurivillius, B., *Acta Chem. Scand. A*, 1980, **34**, 1.
62. Phragmen, G., *J. Inst. Metals*, 1950, **77**, 489.
63. Yan, X.-Y., Private communication.
64. Komura, Y. and Tokunaga, K., *Acta Cryst. B*, 1980, **36**, 1548.

APPENDIX A

A.1. Description of 16-atom SQS structures

Table 7 gives the structural description of the SQS structures used for stoichiometries $x = 1/2$ and $x = 1/4$. The lattice vectors, (ideal) cell-internal positions, and occupations (*A* versus *B* atoms) are given. The SQS at $x = 1/2$ has average pair correlation functions (as discussed in Ref. [42]) equal to the random alloy for all pairs from first- to seventh-nearest-neighbor, whereas the $x = 1/4$ structure first differs from the random alloy at fourth-nearest neighbor.

Table 7. Structural description of the 16-atom SQS structures for $x = 1/2$ and $x = 1/4$[a]

SQS-16 ($x = 1/2$) *AB*	SQS-16 ($x = 1/4$) A_3B
Lattice vectors	
$a_1 = (1.0, 0.5, 0.5)$	$a_1 = (1.0, 0.5, 0.5)$
$a_2 = (0.0, 1.0, -1.0)$	$a_2 = (-0.5, 1.5, 0.0)$
$a_3 = (-1.0, 1.5, 1.5)$	$a_3 = (-0.5, -0.5, 2.0)$
Atomic occupations and positions	
A—(0.5, 0.5, 0.0)	*A*—(0.0, 0.0, 2.0)
A—(0.0, 0.5, 0.5)	*A*—(−0.5, 0.0, 1.5)
A—(0.0, 1.0, 1.0)	*A*—(0.0, 0.5, 1.5)
A—(0.0, 1.5, 0.5)	*A*—(−0.5, 0.5, 1.0)
A—(−0.5, 1.5, 0.0)	*A*—(0.0, 1.5, 0.5)
A—(−0.5, 1.5, 1.0)	*A*—(0.5, 1.0, 0.5)
A—(0.0, 2.0, 1.0)	*A*—(−0.5, 0.5, 2.0)
A—(−0.5, 2.0, 0.5)	*A*—(0.0, 1.0, 2.0)
B—(0.0, 0.0, 0.0)	*A*—(−0.5, 1.0, 1.5)
B—(0.0, 0.5,−0.5)	*A*—(0.0, 1.5, 1.5)
B—(0.5, 1.0,−0.5)	*A*—(0.0, 0.0, 1.0)
B—(0.5, 1.0, 0.5)	*A*—(0.5, 0.5, 1.0)
B—(0.0, 1.0, 0.0)	*B*—(0.0, 0.0, 0.0)
B—(0.5, 1.5, 0.0)	*B*—(0.0, 1.0, 1.0)
B—(−0.5, 1.0, 0.5)	*B*—(−0.5, 1.0, 0.5)
B—(0.0, 1.5, 1.5)	*B*—(0.0, 0.5, 0.5)

[a] Lattice vectors and atomic positions are given in Cartesian coordinates, in units of a, the fcc unit cell vector. Atomic positions are given for the ideal, unrelaxed fcc sites.